NANO LETTERS

Letter

pubs.acs.org/NanoLett

Two-Dimensional Phosphorus Carbide: Competition between sp^2 and sp^3 Bonding

Jie Guan,[†] Dan Liu,[†] Zhen Zhu,[†,‡] and David Tománek*,[†]

[†]Physics and Astronomy Department, Michigan State University, East Lansing, Michigan 48824, United States

[‡]Materials Department, University of California, Santa Barbara, California 93106, United States

Supporting Information

ABSTRACT: We propose previously unknown allotropes of phosphorus carbide (PC) in the stable shape of an atomically thin layer. Different stable geometries, which result from the competition between sp^2 bonding found in graphitic C and sp^3 bonding found in black P, may be mapped onto 2D tiling patterns that simplify categorizing of the structures. Depending on the category, we identify 2D-PC structures that can be metallic, semimetallic with an anisotropic Dirac cone, or direct-gap semiconductors with their gap tunable by in-layer strain.

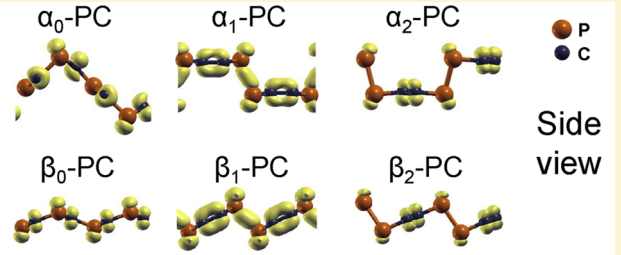

Structure and valence frontier states of 2D phosphorus carbide allotropes

KEYWORDS: *Phosphorus carbide, 2D material, ab initio calculations, electronic structure, Dirac cone, effective mass anisotropy*

There is growing interest in 2D semiconductors, both fundamental and as potential components in flexible, low-power electronic circuitry. A large number of substances with unique advantages and limitations has been studied in this respect, but consensus has not been reached regarding the optimum candidate. Semimetallic graphene with an excellent carrier mobility has received the most attention so far, but all attempts to open up a sizable, robust, and reproducible band gap have failed due to the negative side effects of the different modifications.[1−4] Transition metal dichalchogenides (TMDs) such as MoS_2[5,6] or TcS_2[7] do have a sizable fundamental band gap, but a lower carrier mobility. Recently isolated few-layer films of black phosphorus, including phosphorene monolayers, combine high carrier mobility with a sizable and tunable fundamental band gap,[8,9] but have limited stability in air.[10]

Since both elemental carbon and phosphorus form stable 2D monolayers, which have been studied extensively, it is intriguing to find out, whether the compound phosphorus carbide (PC), also called carbon phosphide, may also be stable as a monolayer and display properties that may even be superior to both constituents. The plausibility of a 2D structure of PC derives from the same 3-fold coordination found both in graphene and phosphorene. On the other hand, the 2D structure will likely suffer from a competition between the planar sp^2 bonding characteristic of graphene and the significantly different nonplanar sp^3 bonding found in phosphorene. The postulated 2D structure of PC with 1:1 stoichiometry is fundamentally different from the amorphous structure observed in deposited thin solid films,[11] the postulated foam-like 3D structure,[12] or the postulated GaSe-like multilayer structures of PC containing C and P with the same sp^3 hybridization.[13,14] On the other hand, 2D allotropes of PC are somehow related to postulated and partly to observed fullerene-like structures of CP_x[15,16] and CN_x,[17−20] and to g-C_3N_4, called graphitic carbon nitride.[21]

In this Letter, based on *ab initio* density functional calculations, we propose previously unknown allotropes of phosphorus carbide in the stable shape of an atomically thin layer. We find that different stable geometries, which result from the competition between sp^2 bonding found in graphitic C and sp^3 bonding found in black P, may be mapped onto 2D tiling patterns that simplify categorizing of the structures. We introduce the structural category N, defined by the number of like nearest neighbors, and find that N correlates with the stability and the electronic structure characteristic. Depending on the category, we identify 2D-PC structures that can be metallic, semimetallic with an anisotropic Dirac cone, or direct-gap semiconductors with their gap tunable by in-layer strain.

Results and Discussion. As mentioned above, all atoms in the 2D-PC allotropes are 3-fold coordinated, similar to the planar honeycomb lattice of graphene. Thus, the structure can be topologically mapped onto a 2D lattice with sites occupied either by P or C atoms. Bisecting all nearest-neighbor bonds by lines yields a 2D tiling pattern, where each triangular tile with a characteristic color represents either a P or a C atom. Next, we define a structural category N for each allotrope, with N given by the number of like nearest neighbors. For $N = 0$, none of the atoms are connected to any like neighbors. Each C or P atom has only one like (C or P) neighbor for $N = 1$, and two like neighbors for $N = 2$. There is no $N = 3$ structure, which would imply a pure carbon or phosphorus lattice. The tiling patterns for different 2D-PC allotropes are shown in Figure 1a−c. A

Received: February 22, 2016
Revised: April 15, 2016
Published: April 18, 2016

DOI: 10.1021/acs.nanolett.6b00767
Nano Lett. 2016, 16, 3247−3252

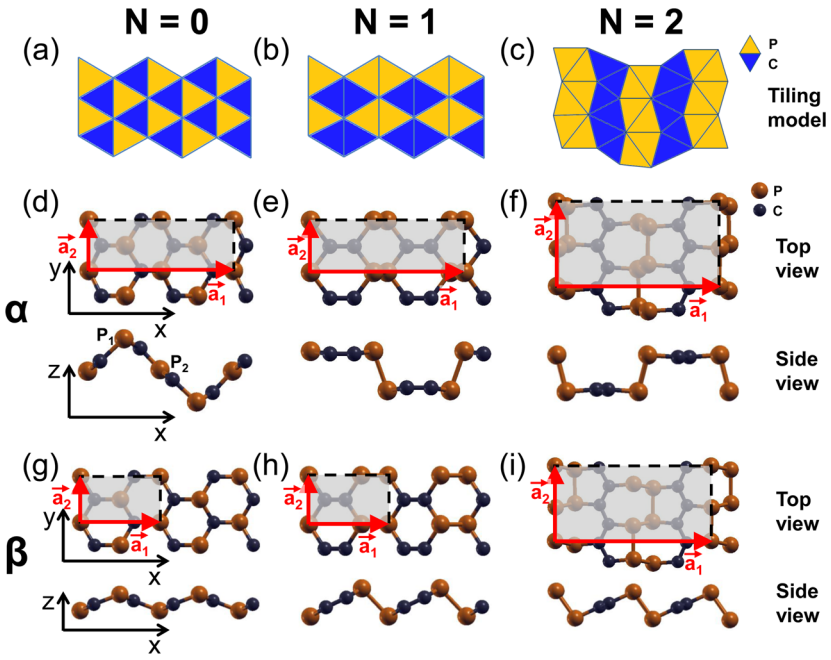

Figure 1. Possible stable structures of an atomically thin PC monolayer, represented by (a–c) tiling patterns and (d–i) by ball-and-stick models in both top and side view. The number of like nearest neighbors defines the structural category *N*. There are two stable allotropes, α and β, for each *N*. The primitive unit cells are highlighted, and the lattice vectors are shown by red arrows. Two inequivalent P sites are distinguished by a subscript in (d).

similar categorization scheme has been used previously to distinguish between different allotropes of 2D phosphorene,[22] where *N* was the number of "like" neighbors either in the upper or lower position within the lattice.

Whereas the tiling pattern is useful for simple categorization, it does not provide information about the nontrivial optimum structure shown in Figure 1d–i, which results from a competition between the favored planar sp^2 hybridization of C and nonplanar sp^3 hybridization of P. The side view of structures displayed in Figure 1 best illustrates that allotropes with the same value of *N* may be structurally different. In analogy to the different postulated phosphorene allotropes,[23,24] we distinguish α_N, which display a black-P-like armchair structure in side view, from β_N phases of PC, which display a blue-P-like (or gray-As-like) zigzag structure in side view, and use the index *N* to identify the structural category.

We start our discussion with $N = 1$ allotropes α_1-PC and β_1-PC, shown in the middle column in Figure 1. According to the definition of *N*, each atom has one neighbor of the same species and two of different species, forming isolated P–P and C–C dimers, as seen in the tiling pattern and the atomic structures. As seen in Figure 2a, the chemical octet rule[25] is satisfied both on C sites in the graphitic sp^2 configuration and on P sites, containing a lone electron pair, in sp^3 configuration, indicating stability. Both allotropes have rectangular unit cells consisting of distorted hexagons. The unit cell of α_1-PC with 8 atoms is larger than that of β_1-PC with four atoms.

In $N = 2$ allotropes α_2-PC and β_2-PC, shown in the right column of Figure 1, each atom has two like neighbors and one unlike neighbor. In the side view, these allotropes look very similar to those of the $N = 1$ category. The main difference becomes apparent in the top view. Whereas $N = 1$ structures contain ethylene-like C_2 units that are interconnected by P_2 dimers, $N = 2$ systems contain contiguous *trans*-polyacetylene-like all-carbon chains that are separated by P-chains. Due to the

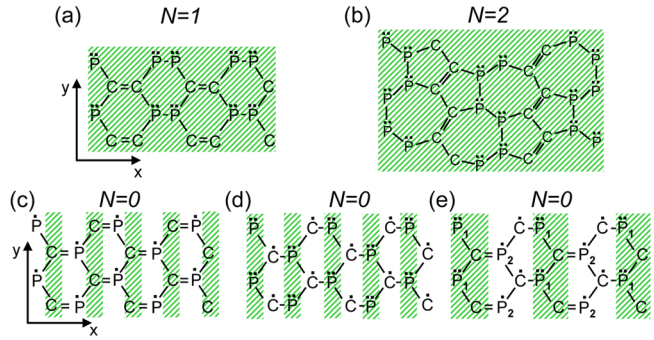

Figure 2. Bonding configuration in (a) $N = 1$, (b) $N = 2$, and (c–e) $N = 0$ category 2D-PC allotropes. Green-shaded regions indicate sites that satisfy the octet rule discussed in the text. Bonding in β_0-PC is characterized by panel (d) and bonding in α_0-PC is described by panel (e).

difference between the locally planar sp^2 bonding of C atoms and locally nonplanar sp^3 bonding of P atoms, and due to the difference between equilibrium C–C and P–P bond lengths, the hexagons found in $N = 1$ structures change to pentagon–heptagon pairs in the optimum $N = 2$ structure resembling pentheptite or haeckelite structures related to graphitic carbon. As seen in Figure 2b, similar to $N = 1$ structures, the chemical octet rule is satisfied on both C and P sites. The lattice of α_2-PC and β_2-PC allotropes contains rectangular unit cells with 16 atoms.

In 2D PC compounds of category $N = 0$, shown in the left column of Figure 1, each atom is surrounded by three unlike neighbors. There is no bonding configuration that would satisfy the octet rules on all sites. The bonding configuration depicted in Figure 2c satisfies the octet rule only at the C sites, whereas the configuration in Figure 2d favors only the P sites. The bonding configuration depicted in Figure 2e contains alternating P–C chains containing P sites with lone electron

DOI: 10.1021/acs.nanolett.6b00767
Nano Lett. 2016, 16, 3247–3252

pairs and C atoms in sp^2 configuration, which satisfy the octet rule, and P−C chains that do not satisfy it. In whatever bonding arrangement, the bonding configuration in $N = 0$ structures is frustrated. As a consequence, the α_0-PC structure converts spontaneously from an initial armchair configuration, similar to α_1-PC and α_2-PC, to the zigzag structure depicted in Figure 1d, with details about the structural transformation discussed in the Supporting Information. The final α_0-PC structure with inequivalent P_1 and P_2 sites reflects the bonding configuration in Figure 2e containing P_1 sites with lone electron pairs and P_2 sites with lone electrons. The β_0-PC structure, depicted in Figure 1g, remains locally stable in the electronic configuration shown in Figure 2d.

Structural characteristics and the binding energy of the different allotropes are summarized in Table 1. Our energy results are obtained using the DFT-PBE functional (including spin polarization where required), which is known to overbind to some degree. We define the cohesive energy per atom, $\langle E_{coh}\rangle$, by dividing the total atomization energy by the total number of atoms, irrespective of species. The energy values in the first rows indicate that, for given N, the α and β phases are almost equally stable, confirming that categorizing structures by the number of like neighbors at any site makes sense in terms of stability. Clearly, $N = 2$ systems are most stable, followed by $N = 1$ and $N = 0$ allotropes. In particular, the cohesive energy of $N = 2$ monolayers exceed the 5.14 eV/atom value of the postulated GaSe-like PC multilayer structures[13,14] by 0.06 eV/atom.

Table 1. Calculated Properties of Different 2D-PC Allotropes[a]

structure	α_0-PC	β_0-PC	α_1-PC	β_1-PC	α_2-PC	β_2-PC
$\langle E_{coh}\rangle$ (eV/atom)	4.80	4.75	5.05	5.06	5.20	5.20
$\langle \Delta E\rangle$ (eV/atom)	−0.40	−0.45	−0.15	−0.14	0.00	0.00
$\lvert\vec{a}_1\rvert$ (Å)	8.41	5.12	8.73	4.76	9.84	10.59
$\lvert\vec{a}_2\rvert$ (Å)	2.94	2.95	2.95	2.95	5.11	5.11
d_{P-P} (Å)			2.36	2.36	2.29	2.29
d_{P-C} (Å)	1.86 (P_1) 1.71 (P_2)	1.78	1.84	1.84	1.85	1.85
d_{C-C} (Å)			1.38	1.38	1.44	1.44

[a] $\langle E_{coh}\rangle$ is the cohesive energy per "average" atom with respect to isolated atoms. $\langle \Delta E\rangle = \langle E_{coh}\rangle - \langle E_{coh,max}\rangle$ describes the relative stability of a system with respect to the most stable structure. $\lvert\vec{a}_1\rvert$ and $\lvert\vec{a}_2\rvert$ are the in-plane lattice constants defined in Figure 1. d_{P-P}, d_{P-C}, and d_{C-C} are the equilibrium bond lengths between the respective species. In α_0-PC, the P_1−C bonds differ from the P_2−C bonds in length.

The lower stability of $N = 0$ systems has been anticipated above, since the octet rule can not be satisfied at all sites. We also note that the α_0 phase is slightly more stable than the β_0 phase of PC. The stability advantage of α_0-PC derives from the larger variational freedom within the unit cell, which allows to distinguish two different P sites (P_1 and P_2), as shown in Figure 1d and Figure 2e. The α_0-PC structure consists of $P_1(sp^3)$−$C(sp^2)$ chains, which obey the octet rule and form stable ridges, alternating with P_2−C chains, which do not obey the octet rule and form terraces.

Additional support for the plausibility of the bonding configuration depicted in Figure 2 comes from the equilibrium bond lengths, which are listed in Table 1. With the exception of $N = 0$ structures, the bond lengths depend primarily on N and are rather insensitive to the phase (α or β). For $N = 1$ and $N = 2$ structures, the C−C bond lengths lie close to the 1.42 Å value in sp^2 bonded graphite (or graphene), and the P−P bond lengths are close to the 2.26−2.29 Å range found in layered black phosphorus (or phosphorene).

As seen in Figure 2a and b, P and C atoms are connected by a single-bond with $d_{P-C} \approx 1.85$ Å in $N = 1$ and $N = 2$ category structures. As suggested above, the bonding is frustrated at least in parts of $N = 0$ structures. In the significantly reconstructed α_0-PC system, depicted in Figure 1d, we can distinguish P_1 sites at ridges from P_2 sites at terraces. The lengths of the three P−C bonds are very similar at each of the these P sites but differ significantly between P_1 and P_2. At P_1 sites that satisfy the octet rule, as seen in Figure 2e, the P_1−C bond length of 1.86 Å is very similar to $N = 1$ and $N = 2$ structures. At P_2 sites, which do not satisfy the octet rule, the frustrated bonds are much shorter with $d_{P-C} = 1.71$ Å. As seen in Figure 1g, there is no reconstruction in the β_0-PC structure. As seen in the corresponding Figure 2c or d, the octet rule is only satisfied at either the P or the C sites. The P−C bonds are frustrated, and their length of 1.78 Å lies in-between the P_1−C and P_2−C bond lengths in α_0-PC.

Results of our DFT-PBE electronic band structure calculations for monolayers of the six proposed PC allotropes are presented in Figure 3.

The electronic band structure and associated density of states (DOS) of $N = 0$ systems is shown in Figure 3a and b. Our results in Figure 3a suggest that α_0-PC is an indirect-gap semiconductor with a band gap of ≈0.7 eV. In stark contrast, the structurally similar β_0-PC allotrope is metallic according to Figure 3b. As suggested earlier, all bonds and electronic configurations are frustrated in β_0-PC, with all C sites engaging only three valence electrons in sp^2-like bonds, leaving one lone electron behind, and the angle at the P ridge being too large for typical sp^3 bonding. This finding, in particular the presence of a nonbonding electron in the $C2p_\perp$ orbital, is seen in the frontier states of β_0-PC that are depicted in the right panel of Figure 2b.

α_0-PC is quite different from β_0-PC, as it contains two inequivalent P and C sites. The P_1 site at the ridge displays the favored sp^3 bonding characteristic and its lone pair orbital is present in the frontier state displayed in the right-hand panel of Figure 3a. In contrast, the bonding is very different at the P_2 site, where the lone pair orbital does not contribute to the frontier state. The flat bonding geometry near this site is reminiscent of sp^2 bonding at the C sites. The added flexibility provided by a larger unit cell allows for additional stabilization of α_0-PC due to the opening of a band gap, with vague analogy to the Peierls instability.

As seen in Figure 3c and d, both α_1-PC and β_1-PC have a direct band gap, which we attribute to the presence of isolated ethylene-like units mentioned above. The two allotropes display a very similar charge distribution in their valence frontier states, which contain the lone pair orbitals on P sites and reflects sp^2 bonding between C sites. The main difference between the two structures is that the 0.4 eV wide gap in α_1-PC is at the Γ point, whereas the 0.3 eV gap in β_1-PC is at the X point. In both structures, the band dispersion is rather anisotropic near the top of the valence and bottom of the conduction band, which causes an anisotropy in the effective mass. We find the effective mass of both electrons and holes to be much smaller along x-direction than along the y-direction, which is reminiscent of the situation in black phosphorene.[8,9]

DOI: 10.1021/acs.nanolett.6b00767
Nano Lett. 2016, 16, 3247−3252

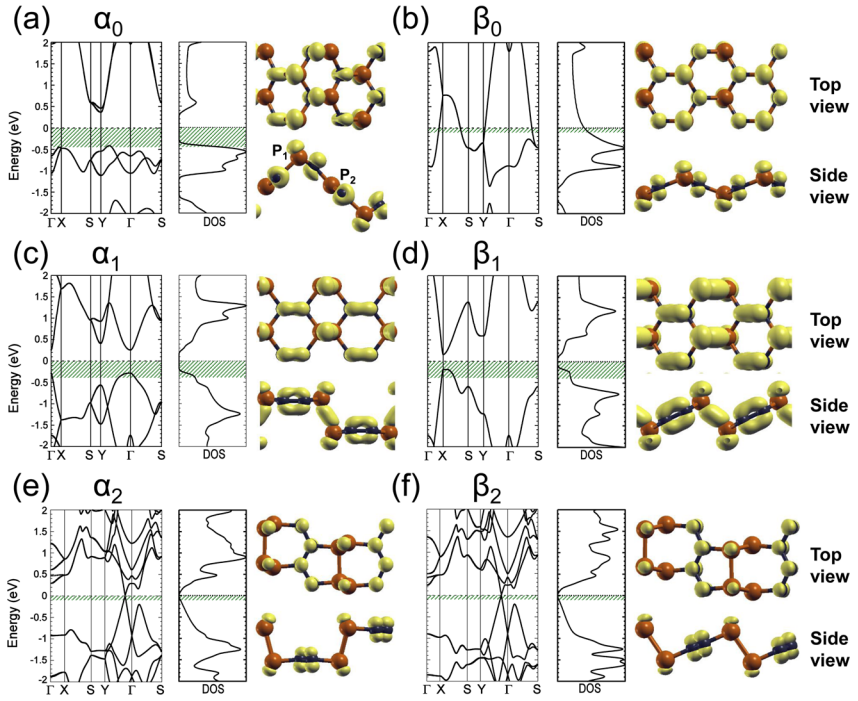

Figure 3. Electronic band structure, density of states (DOS), and charge density ρ_{vc} associated with valence frontier states of α_N and β_N allotropes, where N is the structural category defined in the text and used in Figure 1. The energy range associated with ρ_{vc} is indicated by the green shaded region in the band structure and DOS panels and extends from $E_F - 0.45$ eV $< E < E_F$ for semiconducting α_0-PC in (a), from $E_F - 0.40$ eV $< E < E_F$ for semiconducting α_1-PC in (c) and β_1-PC in (d), and from $E_F - 0.10$ eV $< E < E_F$ for metallic β_0-PC in (b), and for semimetallic α_2-PC in (e) and β_2-PC in (f). For each system, isosurface plots of ρ_{vc} are displayed in the right-side panels and superposed with ball-and-stick models of the structure in top and side view. The isosurface values of ρ_{vc} are 1.0×10^{-3} e/Å^3 in (a), 2.0×10^{-3} e/Å^3 in (b), 0.5×10^{-3} e/Å^3 in (c) and (d), and 0.5×10^{-4} e/Å^3 in (e) and (f).

The effective mass anisotropy offers a significant advantage in transport, since it combines high mobility of carriers with a large DOS near the band edges.

According to Figure 3e and f, also the two $N = 2$ allotropes, α_2-PC and β_2-PC, share a very similar band structure, DOS, and frontier orbitals due to structural similarities. The electronic structure of these systems is nevertheless very different from the other two categories, chiefly due to the presence of *trans*-polyacetylene-like chains mentioned above. Both α_2-PC and β_2-PC display a Dirac cone at the Fermi level, at a crystal momentum between Γ and Y. As mentioned before, the distinguishing feature of $N = 2$ structures is the alternation between chains consisting of pure P or pure C atoms. Figure 2b indicates that all P sites have occupied lone pair orbitals, which are also reflected in the frontier states. The P chains form ridges within the structure, with bond angles characteristic of sp^3 bonding found in black phosphorus. The structure of the carbon chains, also illustrated in Figure 2b, resembles that of conjugated *trans*-polyacetylene or graphene with sp^2 bonding, and the presence of C2$p_\perp$ orbitals in the frontier states is clearly seen in the right-side panels of Figure 3e and f. Differences between equilibrium bond length and bond angles of the P and C chains are accommodated by introducing pentagon-heptagon pairs. The conjugation within C chains and their suppressed dimerization caused by their bonding to adjacent P chains lies behind the formation of the Dirac cone. Due to the strong anisotropy in the system, caused by the direction of the *trans*-polyacetylene-like chains, the Dirac cone is anisotropic in the plane of the layer. We have found that uniaxial strain may be used to eliminate the anisotropy of the Dirac cone, but will also change the location of the Dirac point along the Γ−Y line. More information about the Dirac cone is provided in the Supporting Information.

Even though DFT-PBE calculations notoriously underestimate the fundamental band gap between occupied and unoccupied states, the calculated dispersion $E(\mathbf{k})$ of individual bands is believed to closely resemble experimental values. For the sake of comparison, we have also performed DFT-HSE06[26,27] calculations with a hybrid exchange-correlation functional for the same structures. As seen in the Supporting Information, our DFT-PBE and DFT-HSE06 results are closely related. In particular, DFT-HSE06 opens the band gap in semiconducting α_0-PC, α_1-PC, and β_1-PC structures, but keeps the metallic character of β_0-PC and the semimetallic character of α_2-PC and β_2-PC.

Similar to other nonplanar 2D systems like phosphorene, PC is susceptible to even minute in-plane stress, which can cause major distortions in the geometry, affecting the electronic structure and bonding. To quantify this effect, we have determined the effect of tensile and compressive strain on the stability and the fundamental band gap in the different PC allotropes and present the results in Figure 4. We have considered uniaxial strain along the x- and the y-direction, defined in Figure 1. Since all allotropes discussed here are nonplanar, applying in-layer strain changes the effective thickness of the layers and vice versa. As expected, layer thickness is reduced under tensile strain and increased under compressive strain. For strain values below 5%, we have observed changes in layer thickness of up to 10%. The distinct structural anisotropy, best seen in the side views, translates into a distinct anisotropy of the strain energy with respect to the strain direction, shown in Figure 4a. Similar to black

DOI: 10.1021/acs.nanolett.6b00767
Nano Lett. 2016, 16, 3247−3252

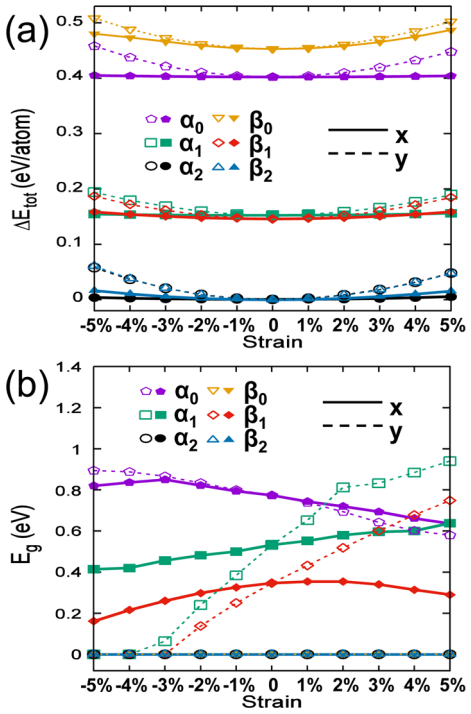

Figure 4. Effect of uniaxial in-layer strain on (a) the relative binding energy ΔE_{tot} and (b) the fundamental band gap in different PC allotropes. Results for α_0-PC, β_0-PC, α_1-PC, β_1-PC, α_2-PC, and β_2-PC are distinguished by color and symbols. Results for strain in the *x*-direction, defined in Figure 1, are shown by solid lines and for strain in the *y*-direction by dashed lines.

phosphorene, the system appears soft when strained along the *x*-direction normal to the ridges and valleys, whereas it is much stiffer when distorted along the *y*-direction. We find the α phase to be particularly soft in the *x*-direction, with compressive or tensile strain requiring $\Delta E \lesssim 5$ meV/atom in strain energy.

The dependence of the fundamental band gap on the in-layer strain, as obtained by our DFT-PBE calculations, is shown in Figure 4b. We find that compression along the soft *x*-direction does not affect the band gap much, quite unlike what is expected to occur in black phosphorene.[8] This is quite different from our results for strain along the stiffer *y*-direction. There, we observe the fundamental band gap to disappear at compressive strain exceeding 4% for α_1-PC and 3% for β_1-PC. We also find that the metallic character of β_0-PC and semimetallic character of α_2-PC and β_2-PC are not affected by tensile or compressive strains up to 5% applied along the *x*- or the *y*-direction. Since vertical strain causing a 10% reduction of the layer thickness is equivalent to an effective tensile in-layer strain below 5%, we can judge its effect on the electronic structure based on the above findings.

Even though the cohesive energy of the 2D structures presented here exceeds that of previously discussed PC systems, the calculated cohesive energy of per formula unit still falls 0.54 eV short of the sum of the cohesive energies of pure black phosphorene, 3.27 eV, and pure graphene, 7.67 eV. Even though the PC allotropes discussed here are all stable, as seen in the vibration spectra presented in the Supporting Information, the slight energetic preference for pure components in favor of the PC compound should offer challenges in the synthesis. We believe that recent advances in supramolecular assembly may solve this problem. Similar to our requirements, precisely designed structures including graphdiyne,[28,29] graphene nanoribbons,[30] and carbon nanotubes[31] have been assembled using wet chemical processes from specific molecular precursors. In the same way, we expect that the postulated 2D-PC structures may be formed of proper molecular precursors that contain sp^2 bonded carbon and sp^3 bonded phosphorus.

Conclusions. In conclusion, we have performed *ab initio* density functional calculations and identified previously unknown allotropes of phosphorus carbide (PC) in the stable shape of an atomically thin layer. We found that different nonplanar stable geometries, which result from the competition between sp^2 bonding found in graphitic C and sp^3 bonding found in black P, may be mapped onto 2D tiling patterns that simplify categorizing of the structures. We have introduced the structural category *N*, defined by the number of like nearest neighbors ranging from 0 to 2, and found that *N* correlates with the stability and the electronic structure characteristic. We found structures of the $N = 0$ category to be either metallic, or to reconstruct spontaneously to a more stable structure with a larger unit cell and a sizable fundamental gap. Systems of the $N = 1$ category are more stable than $N = 0$ systems, display a significant, direct band gap and a significant anisotropy of the effective mass of carriers. Category $N = 2$ systems are the most stable of all, are semimetallic, and display an anisotropic Dirac cone at the Fermi level. Due to their nonplanar character, all systems can sustain in-layer strain at little energy cost. The fundamental band gap is not very sensitive to strain in most systems with the exception of $N = 1$ allotropes, where it closes upon applying compressive strain of $\lesssim$5% along the ridges and valleys.

Methods. We use *ab initio* density functional theory (DFT) as implemented in the SIESTA[32] code to obtain insight into the equilibrium structure, stability, and electronic properties of 2D-PC allotropes reported in the main manuscript. Periodic boundary conditions are used throughout the study, with monolayers represented by a periodic array of slabs separated by a 15 Å thick vacuum region. We use the Perdew–Burke–Ernzerhof (PBE)[33] exchange-correlation functional, norm-conserving Troullier-Martins pseudopotentials,[34] and a double-ζ basis including polarization orbitals. The reciprocal space is sampled by a fine grid[35] of $8 \times 12 \times 1$ *k*-points in the Brillouin zone of the primitive unit cell of 4 atoms or its equivalent in supercells. SIESTA calculations use a mesh cutoff energy of 180 Ry to determine the self-consistent charge density, which provides us with a precision in total energy of $\lesssim$2 meV/atom. All geometries have been optimized using the conjugate gradient method,[36] until none of the residual Hellmann–Feynman forces exceeded 10^{-2} eV/Å. Since the fundamental band gap is usually underestimated in DFT-PBE calculations, we have resorted to the HSE06[26,27] hybrid exchange-correlation functional, as implemented in the VASP[37−40] code, to get a different (possibly superior) description of the band structure. We use 500 eV as energy cutoff and the default mixing parameter value $\alpha = 0.25$ in these studies. DFT-PBE and DFT-HSE06 band structure results are compared in the Supporting Information.

■ ASSOCIATED CONTENT

Supporting Information

The Supporting Information is available free of charge on the ACS Publications website at DOI: 10.1021/acs.nanolett.6b00767.

DOI: 10.1021/acs.nanolett.6b00767
Nano Lett. 2016, 16, 3247−3252

Geometry transformation pathway and corresponding changes in the electronic band structure of α_0-PC, details of the electronic band structure in all PC allotropes, and the phonon band structure of β_0-PC and β_1-PC (PDF) Reconstruction process of α_0-PC (AVI)

AUTHOR INFORMATION

Corresponding Author

*E-mail: tomanek@pa.msu.edu.

Notes

The authors declare no competing financial interest.

ACKNOWLEDGMENTS

We thank Teng Yang and Baojuan Dong for their help in performing the HSE calculations and acknowledge useful discussions with Garrett B. King. This study was supported by the NSF/AFOSR EFRI 2-DARE grant number EFMA-1433459. Computational resources have been provided by the Michigan State University High Performance Computing Center.

REFERENCES

(1) Elias, D. C.; Nair, R. R.; Mohiuddin, T. M. G.; Morozov, S. V.; Blake, P.; Halsall, M. P.; Ferrari, A. C.; Boukhvalov, D. W.; Katsnelson, M. I.; Geim, A. K.; Novoselov, K. S. *Science* **2009**, *323*, 610−613.

(2) Han, M. Y.; Özyilmaz, B.; Zhang, Y.; Kim, P. *Phys. Rev. Lett.* **2007**, *98*, 206805.

(3) Nakada, K.; Fujita, M.; Dresselhaus, G.; Dresselhaus, M. S. *Phys. Rev. B: Condens. Matter Mater. Phys.* **1996**, *54*, 17954−17961.

(4) Wimmer, M.; Adagideli, I.; Berber, S.; Tomanek, D.; Richter, K. *Phys. Rev. Lett.* **2008**, *100*, 177207.

(5) Radisavljevic, B.; Radenovic, A.; Brivio, J.; Giacometti, V.; Kis, A. *Nat. Nanotechnol.* **2011**, *6*, 147−150.

(6) Fuhrer, M. S.; Hone, J. *Nat. Nanotechnol.* **2013**, *8*, 146−147.

(7) Weck, P. F.; Kim, E.; Czerwinski, K. R. *Dalton Trans.* **2013**, *42*, 15288−15295.

(8) Liu, H.; Neal, A. T.; Zhu, Z.; Luo, Z.; Xu, X.; Tomanek, D.; Ye, P. D. *ACS Nano* **2014**, *8*, 4033−4041.

(9) Li, L.; Yu, Y.; Ye, G. J.; Ge, Q.; Ou, X.; Wu, H.; Feng, D.; Chen, X. H.; Zhang, Y. *Nat. Nanotechnol.* **2014**, *9*, 372−377.

(10) Wood, J. D.; Wells, S. A.; Jariwala, D.; Chen, K.-S.; Cho, E.; Sangwan, V. K.; Liu, X.; Lauhon, L. J.; Marks, T. J.; Hersam, M. C. *Nano Lett.* **2014**, *14*, 6964−6970.

(11) Furlan, A.; Gueorguiev, G.; Czigány, Z.; Darakchieva, V.; Braun, S.; Correia, M.; Högberg, H.; Hultman, L. *Thin Solid Films* **2013**, *548*, 247−254.

(12) Hart, J. N.; Allan, N. L.; Claeyssens, F. *Phys. Chem. Chem. Phys.* **2010**, *12*, 8620−8631.

(13) Claeyssens, F.; Fuge, G. M.; Allan, N. L.; May, P. W.; Ashfold, M. N. R. *Dalton Trans.* **2004**, 3085−3092.

(14) Zheng, J.-C.; Payne, M. C.; Feng, Y. P.; Lim, A. T.-L. *Phys. Rev. B: Condens. Matter Mater. Phys.* **2003**, *67*, 153105.

(15) Gueorguiev, G.; Furlan, A.; Högberg, H.; Stafström, S.; Hultman, L. *Chem. Phys. Lett.* **2006**, *426*, 374−379.

(16) Furlan, A.; Gueorguiev, G.; Högberg, H.; Stafström, S.; Hultman, L. *Thin Solid Films* **2006**, *515*, 1028−1032.

(17) Gueorguiev, G.; Neidhardt, J.; Stafström, S.; Hultman, L. *Chem. Phys. Lett.* **2005**, *401*, 288−295.

(18) Gueorguiev, G.; Neidhardt, J.; Stafström, S.; Hultman, L. *Chem. Phys. Lett.* **2005**, *410*, 228−234.

(19) Sjöström, H.; Stafström, S.; Boman, M.; Sundgren, J.-E. *Phys. Rev. Lett.* **1995**, *75*, 1336−1339.

(20) Neidhardt, J.; Hultman, L.; Abendroth, B.; Gago, R.; Möller, W. *J. Appl. Phys.* **2003**, *94*, 7059−7066.

(21) Thomas, A.; Fischer, A.; Goettmann, F.; Antonietti, M.; Muller, J.-O.; Schlogl, R.; Carlsson, J. M. *J. Mater. Chem.* **2008**, *18*, 4893−4908.

(22) Guan, J.; Zhu, Z.; Tománek, D. *ACS Nano* **2014**, *8*, 12763−12768.

(23) Zhu, Z.; Tománek, D. *Phys. Rev. Lett.* **2014**, *112*, 176802.

(24) Guan, J.; Zhu, Z.; Tománek, D. *Phys. Rev. Lett.* **2014**, *113*, 046804.

(25) Langmuir, I. *J. Am. Chem. Soc.* **1919**, *41*, 868−934.

(26) Heyd, J.; Scuseria, G. E.; Ernzerhof, M. *J. Chem. Phys.* **2003**, *118*, 8207−8215.

(27) Krukau, A. V.; Vydrov, O. A.; Izmaylov, A. F.; Scuseria, G. E. *J. Chem. Phys.* **2006**, *125*, 224106.

(28) Li, G.; Li, Y.; Liu, H.; Guo, Y.; Li, Y.; Zhu, D. *Chem. Commun.* **2010**, *46*, 3256−3258.

(29) Liu, H.; Xu, J.; Li, Y.; Li, Y. *Acc. Chem. Res.* **2010**, *43*, 1496−1508.

(30) Cai, J.; Ruffieux, P.; Jaafar, R.; Bieri, M.; Braun, T.; Blankenburg, S.; Muoth, M.; Seitsonen, A. P.; Saleh, M.; Feng, X.; Mullen, K.; Fasel, R. *Nature* **2010**, *466*, 470−473.

(31) Sanchez-Valencia, J. R.; Dienel, T.; Groning, O.; Shorubalko, I.; Mueller, A.; Jansen, M.; Amsharov, K.; Ruffieux, P.; Fasel, R. *Nature* **2014**, *512*, 61−64.

(32) Artacho, E.; Anglada, E.; Dieguez, O.; Gale, J. D.; Garcia, A.; Junquera, J.; Martin, R. M.; Ordejon, P.; Pruneda, J. M.; Sanchez-Portal, D.; Soler, J. M. *J. Phys.: Condens. Matter* **2008**, *20*, 064208.

(33) Perdew, J. P.; Burke, K.; Ernzerhof, M. *Phys. Rev. Lett.* **1996**, *77*, 3865−3868.

(34) Troullier, N.; Martins, J. L. *Phys. Rev. B: Condens. Matter Mater. Phys.* **1991**, *43*, 1993−2006.

(35) Monkhorst, H. J.; Pack, J. D. *Phys. Rev. B* **1976**, *13*, 5188−5192.

(36) Hestenes, M. R.; Stiefel, E. *J. Res. Natl. Bur. Stand.* **1952**, *49*, 409−436.

(37) Kresse, G.; Furthmüller, J. *Phys. Rev. B: Condens. Matter Mater. Phys.* **1996**, *54*, 11169−11186.

(38) Kresse, G.; Hafner, J. *Phys. Rev. B: Condens. Matter Mater. Phys.* **1993**, *47*, 558−561.

(39) Kresse, G.; Hafner, J. *Phys. Rev. B: Condens. Matter Mater. Phys.* **1994**, *49*, 14251−14269.

(40) Kresse, G.; Joubert, D. *Phys. Rev. B: Condens. Matter Mater. Phys.* **1999**, *59*, 1758−1775.

DOI: 10.1021/acs.nanolett.6b00767
Nano Lett. 2016, 16, 3247−3252